

1 Accepted to The Cryosphere, 16 October 2014;
2 Contact: T. Scambos, teds@nsidc.org, 303/492-1113

3
4
5
6 **Detailed ice loss pattern in the northern Antarctic Peninsula:**
7 **widespread decline driven by ice front retreats**

8
9
10 Ted A. Scambos¹, Etienne Berthier², Terry Haran¹, Christopher A. Shuman³, Alison J.
11 Cook⁴, Stefan R. M. Ligtenberg⁵, and Jennifer Bohlander¹

12
13 ¹National Snow and Ice Data Center (NSIDC), University of Colorado at Boulder, Boulder CO
14 80303 USA

15 ²Laboratoire d'Etudes en Géophysique et Océanographie Spatiales, Centre National de la
16 Recherche Scientifique (LEGOS CNRS), Université de Toulouse, Toulouse 31400 France

17 ³University of Maryland, Baltimore County, Joint Center for Earth Technology (UMBC JCET)
18 at NASA Goddard Space Flight Center, Greenbelt, MD 20771 USA

19 ⁴Department of Geography, Swansea University, Swansea SA2 8PP UK

20 ⁵Institute for Marine and Atmospheric Research Utrecht (IMAU), Utrecht 3508 TA
21 Netherlands

22
23
24 Corresponding author: T.A. Scambos (National Snow and Ice Data Center, University of
25 Colorado, Boulder, 1540 30th Street Bldg. RL-2, Boulder CO 80303, teds@nsidc.edu, +1-
26 303-492-1113).

27
28

29 **Abstract**

30 The northern Antarctic Peninsula (nAP, <66°S) is one of the most rapidly changing
31 glaciated regions on Earth, yet the spatial patterns of its ice mass loss at the glacier
32 basin scale have to date been poorly documented. We use satellite laser altimetry
33 and satellite stereo-image topography spanning 2001-2010, but primarily 2003-
34 2008, to map ice elevation change and infer mass changes for 33 glacier basins
35 covering the mainland and most large islands in the nAP. Rates of ice volume and ice
36 mass change are $27.7 \pm 8.6 \text{ km}^3 \text{ a}^{-1}$ and $24.9 \pm 7.8 \text{ Gt a}^{-1}$, equal to 0.73 m a^{-1} w.e. for the
37 study area. Mass loss is highest for eastern glaciers affected by major ice shelf
38 collapses in 1995 and 2002, where twelve glaciers account for 60% of the total
39 imbalance. However, losses at smaller rates occur throughout the nAP, at both high
40 and low elevation, despite increased snow accumulation along the western coast
41 and ridge crest. We interpret the widespread mass loss to be driven by decades of
42 ice front retreats on both sides of the nAP, and extended throughout the ice sheet
43 due to the propagation of kinematic waves triggered at the fronts into the interior.

44 (194 words)

45 **Index terms:**

46 Ice Shelves; Glaciers; Mass Balance; Remote Sensing; Instruments and techniques

47 **Keywords:**

48 Antarctic Peninsula; ICESat; DEM differencing; Larsen B; Larsen A; Prince Gustav
49
50
51

52 **1 Introduction**

53 The nAP is one of two areas of the Antarctic Ice Sheet showing major mass loss, the
54 other being the Amundsen Sea coast of West Antarctica's ice sheet. Previous studies
55 have shown large negative mass imbalances and significant elevation losses for the
56 nAP (*Ivins et al.*, 2011; *Shepherd et al.*, 2012; *Luthcke et al.*, 2013; *Sasgen et al.*, 2013;
57 *McMillan et al.*, 2014). However, in general these studies have not resolved the
58 spatial distribution of mass imbalance in detail, nor attempted to link patterns of ice
59 loss to processes responsible for the loss. Studies based on gravitational change
60 detection using the Gravity Recovery and Climate Experiment satellite system
61 (GRACE) have an inherent spatial resolution of roughly 250 km scale (*Ivins et al.*,

2011; *Luthcke et al.*, 2013; *Sasgen et al.*, 2013), far larger than the scale of the nAP individual glacier basins and islands. Past altimetry-based studies (*Pritchard et al.*, 2009; *Flament and Rémy*, 2012; *Shepherd et al.*, 2012; *McMillan et al.*, 2014) suffer from either sparse coverage or slope correction issues, or both, due to the steep terrain in the nAP. In the published assessments based on laser altimetry (*Shepherd et al.*, 2012), broad assumptions and large extrapolations are required to interpolate the data across the dissected and rugged Peninsula region. Mass budget methods (*Rignot et al.*, 2004, 2008; *Rott et al.*, 2011; *Shepherd et al.*, 2012), which aim to difference outflowing ice flux and surface mass balance (SMB) for each glacier basin have to date shown results that are difficult to reconcile with other studies of the same glaciers (*Shuman et al.*, 2011; *Berthier et al.*, 2012). This is primarily due to spatially coarse SMB estimates from models or field measurements, difficulties in estimating the cross-sectional area of the glaciers, and differences in the span of time used to estimate ice flux changes (*Berthier et al.*, 2012).

The goal of this study is to determine the spatial pattern of ice elevation changes in the nAP, improve estimates of mass balance for the region, and study the relationship of mass balance with ice shelf collapse and ice front retreats in the area. In light of known climate-related changes in the region, such as increasing surface air temperatures and surface melting, regional sea ice decline, and increasing accumulation (e.g., *Mulvaney et al.* 2012; *Zagorodnov et al.*, 2012; *Stammerjohn et al.*, 2008; *Lenaerts et al.*, 2012; *Barrand et al.*, 2013), our study reveals a pattern of ice mass loss in space and (we infer) in time that may be similar to the characteristics of mass loss in other areas of Antarctica in the coming century.

2 Methods

Our study combines satellite stereo-image digital elevation model differencing (dDEM) with repeat-track laser altimetry from the Ice, Cloud and land Elevation Satellite (ICESat; *Schutz et al.*, 2005), with the objective of providing an assessment of surface elevation change resolved at the scale of the major glacier catchments. We use stereo-image data from the Advanced Spaceborne Thermal Emission and

93 Reflection Radiometer (ASTER; *Fujisada et al.*, 2005) and Satellite Pour
94 l'Observation de la Terre 5 (SPOT5; *Korona et al.*, 2009). Eight satellite stereo-image
95 data sets from the ASTER sensor, and six from the SPOT-5 Haute Résolution
96 Stéréoscopique (HRS) sensor (Table S1 and Figure S1) were processed using
97 previously published methods (*Shuman et al.*, 2011; *Berthier et al.*, 2012; *Gardelle et*
98 *al.*, 2013).

99
100 For the ICESat repeat-track data (Release 633), we used 26 ground tracks from the
101 91-day-repeat orbit crossing the nAP and major ice-covered islands for the high-
102 energy laser campaigns (ICESat Laser 2A through Laser 3J, September 2003 – March
103 2008; *Shuman et al.*, 2006; *Zwally et al.*, 2012). Cross-track elevation adjustment and
104 along-track filtering are used to improve measurement quality, based on surface
105 slopes (not elevations) derived from a recent Antarctic Peninsula DEM (*Cook et al.*,
106 2012). We first eliminated ICESat profile tracks more than 300 meters from the
107 reference track position, and sections where the absolute slope from the gridded
108 DEM was $> \pm 10\%$ slope (or $\pm 5.7^\circ$) for the reference track or measurement track
109 location, or areas where the absolute difference between along-track slopes of the
110 measurement track and reference track exceeded 5% (or $\pm 2.86^\circ$). We further
111 required the ICESat elevation data to be within 50 m (vertically) of the
112 corresponding interpolated DEM elevation. All elevations are referenced to the
113 EGM96 geoid datum. To migrate the measurement track data to the reference track
114 and compare elevations, we identified reference track 'stations' every 43.75 m along
115 the reference track (one-fourth the distance between ICESat altimetry shot locations
116 along track). We then applied an elevation correction based on the difference
117 between the interpolated gridded DEM elevation at the nearest reference track
118 station and the ICESat track data point. ICESat campaign data were compared by
119 differencing their migrated elevations, divided by the time in years between dates of
120 track acquisition. To reduce effects of possible seasonal variations in elevation, we
121 compared only near-integer-year separated repeat profiles, e.g., data from
122 campaigns 2A to 3A (~October, ~1 year apart) or 3B to 3H (~March, ~2 years
123 apart).

124

125 To evaluate different processes in elevation and ice mass change, we treat regions
126 above and below 1000 m above sea level (a.s.l.) separately for each of 33 drainage
127 basins. This is the approximate elevation of an extensive escarpment in the nAP
128 separating plateau areas from individual glacier cirques. Above 1000 m a.s.l., and for
129 islands without sufficient dDEM coverage (Robertson Is., Snow Hill Is., and Joinville,
130 Dundee, and D'Urville islands; Figure 1), the rate of elevation change (dH/dt) is
131 determined from satellite laser altimetry alone. In smooth high elevation areas,
132 correlation of satellite stereo-images often fails due to a lack of high-contrast
133 surface features of sufficient horizontal scale (tens of meters). Below 1000 m a.s.l., a
134 hypsometric interpolation method was applied to individual glacier basins to extend
135 dDEMs and ICESat dH/dt measurements to areas not directly measured. ICESat
136 dH/dt was weighted 10-fold relative to dDEM dH/dt to prevent small dDEM data
137 areas from dominating the weighted dH/dt mapping, and to better utilize the higher
138 accuracy of individual ICESat-based measurements. We used the relationship

139

$$140 \quad dH/dt_{\text{hyps}} = (dH/dt_{\text{DEM}} * (N_{\text{DEM}}/e_{\text{DEM}}) + dH/dt_{\text{ICESat}} * (N_{\text{ICESat}}/e_{\text{ICESat}})) / ((N_{\text{DEM}}/e_{\text{DEM}}) + (N_{\text{ICESat}}/e_{\text{ICESat}})) \quad (1)$$

141

142 where N is the number of measurements within an elevation band (i.e., the number
143 of 50 m grid cells for the dDEMs; or reference track site locations at 43.75 m spacing
144 for ICESat) and e is an inverse weighting of the measurement methods. For dDEMs
145 we used a weight of 1, and for ICESat, we used 0.1. This allowed the fewer but more
146 accurate ICESat-based measurements to contribute to the final result in basins with
147 extensive dDEM coverage. In several areas, ICESat data were available in regions not
148 well covered by dDEM results (see Figure S2).

149

150 We also estimate the above-flotation mass loss of grounded-ice areas that retreated
151 at least 2 km² during the study interval (2001-2010), as identified by image
152 mapping (Cook *et al.*, 2005; Cook and Vaughan, 2010). To estimate the volume and
153 mass loss represented by these areas we mapped the area of retreat during our
154 study period (2001-2010) and half the mean elevation loss rate observed just above

155 the area of grounded ice retreat. This represents an assumption that the vertical
156 elevation change rate of the retreated ice was identical to the region just upstream
157 of the loss area, and that the time of ice front retreat (e.g., when the ice calved and
158 drifted away) was midway through the study period.

159

160 Errors for our assessment of dH/dt (Tables 1 and S2), are based on past analysis of
161 the dDEM method (*Shuman et al., 2011; Berthier et al., 2012*), on inter-comparisons
162 of the two methods at sites having both dDEM and ICESat measurements, and on
163 crossover analysis of ICESat cross-track-corrected data (Table S4). Past analysis for
164 this region suggests that dDEM methods using mixed ASTER and SPOT5 imagery
165 can have a ± 5 m uncertainty for individual glacier basins, i.e. ~ 1 m a^{-1} given a 5-yr
166 time separation between DEMs. However, examining our ICESat and dDEM dH/dt at
167 sites with both measurements (6158 sites) shows that the methods differ by just
168 ~ 0.3 m a^{-1} overall, a difference that ranges between 0.07 to 0.75 m a^{-1} over various
169 sub-sets of our measurements (Table S4). This is in agreement with our previous
170 study that showed reduced errors when dDEM results are averaged over basin-scale
171 areas (*Berthier et al., 2012*). Seven crossover sites with slope-corrected ICESat
172 dH/dt measurements show good agreement with the dDEM measurements at the
173 same locations (mean offset of $+0.05$ m a^{-1}).

174

175 Errors in the ICESat cross-track correction for dH/dt are more dependent on slope
176 errors in the Cook et al. (2012) DEM and not its absolute elevation accuracy.
177 Assuming our selection criteria eliminated regions of significant error in the DEM,
178 we estimate that across-track or along-track slopes in the Cook et al. (2012) DEM
179 are accurate to within $\pm 0.5^\circ$ over a length scale of 300 m, or ± 8.7 m km^{-1} . A test of
180 this was conducted by comparing the Cook et al. (2012) DEM slopes with a DEM
181 acquired in 2009 by the NASA Land, Vegetation, and Ice Sensor (LVIS) airborne laser
182 altimeter, covering about 20% of the study region. This showed that the mean
183 difference in along-track slope in the overlap region was $0.06 \pm 1.2^\circ$ when our
184 criteria are applied to both data sets. For laser altimetry measurements alone, our
185 inferred mean slope error of $\pm 0.5^\circ$ implies a mean laser measurement pair cross-

186 track correction error of ± 1.31 m (assuming a mean cross-track distance of 150 m).
187 We assume this error is randomly distributed when averaging over a glacier basin.
188 Thus for the average of 20 measurement sites, the mean error is < 25 cm. Since laser
189 measurement pairs may have 1 to 4 years separation in time, and many have
190 multiple measurements at a single site (see Figure S2), our overall mean error in
191 elevation change rate is significantly less than this. Additionally, the majority of the
192 basins we consider have many more than 20 measurement sites (Table S2).

193

194 Considering all sources of error, and variations in the time-span of measurements
195 for dDEM and ICESat measurements, data density variations for the basins, and the
196 strong agreement between these independent altimetric methods, we adopt a mean
197 error of ± 0.15 m a^{-1} for regions of laser altimetry measurement alone (above 1000
198 m a.s.l.), and ± 0.3 m a^{-1} for our dDEM plus altimetry measurements (below 1000 m
199 a.s.l.) and the glacier basins, islands, and sub-basins without laser altimetry. Errors
200 for volume and mass change determinations thus scale with area.

201

202 **3 Results**

203 An overview of our results is shown in Figure 2 and Table 1, and detailed basin-by-
204 basin values are provided in supplementary Table S2. The results show that basins
205 impacted by recent ice shelf loss and ice front retreat have very high rates of change,
206 but also indicate that few areas — high or low, east or west — have positive dH/dt .
207 Recent ice-shelf loss (ISL) basins (losses since 1986, and particularly in 1995 and
208 2002), all on the eastern side of the nAP, and four smaller glaciers with recent
209 grounded ice front loss (IFL; losses since 2000) on the western and northeastern side
210 of the nAP, show a characteristic pattern of very high elevation loss rates just
211 upstream of the ice front but far lower elevation loss rates at high elevation. Mean
212 elevation change for areas below 1000 m a.s.l. at 12 eastern-side ISL glacier basins
213 (or sub-basins) is -2.6 m a^{-1} (range, $+0.4$ to -5.8 m a^{-1}) and -2.2 m a^{-1} (-2.0 to -2.7 m a^{-1})
214 for the four western-side and northeastern IFL sub-basins experiencing recent ice
215 front retreat (> 2 km² since 2000). At elevations > 1000 m, elevation loss in the
216 eastern ISL basins is small (mean, -0.10 m a^{-1} ; range $+0.35$ to -0.54 m a^{-1}). Glacier

217 systems on the western nAP coast and the western islands below 1000 m a.s.l.,
218 excluding the recent IFL regions, are changing at various rates (typically $\sim -0.15 \text{ m a}^{-1}$,
219 1 , range $+0.7$ to -1.6 m a^{-1}). However, western-side basins are losing elevation at
220 significant rates above 1000 m a.s.l. (mean, -0.59 m a^{-1} ; range -0.25 to -1.30 m a^{-1}). In
221 terms of mean water equivalent layer, the overall study area has lost an average of
222 0.73 m a^{-1} w.e. during the study period; the western glaciers (basins 1-11) averaged
223 0.33 m a^{-1} w.e., and eastern glacier systems impacted by ice shelf loss (basins 19, 21-
224 25, 26b, 27-30, and 31a) averaged 1.48 m a^{-1} w.e. elevation loss.

225

226 We examine the rates of surface elevation change and cumulative ice volume change
227 as they vary with altitude for three sub-regions of the study area in Figure 3. The
228 patterns of elevation change with altitude illustrate the differences between the
229 western-side glacier and island regions and the eastern-side ISL areas, and also
230 highlight the bi-modal hypsometry pattern characteristic of the nAP. Eastern-side
231 ISL areas show dramatically decreasing elevation, and large volume changes at low
232 elevations, but relatively small elevation losses in the upper-most catchment areas
233 (Figure 3c-d). Western-side glaciers show negative rates of elevation change at all
234 elevations, and a steady cumulative volume decrease rate with altitude. The major
235 glaciers of Scar Inlet Ice Shelf, the lone remaining large ($>50 \text{ km}^2$) ice shelf in the
236 study area with significant tributary glaciers, show a unique pattern of ice loss
237 at low elevation and some areas of thickening at altitude. We believe this is likely
238 the pattern of elevation change present for the eastern nAP ISL glacier systems in
239 the years immediately prior to shelf disintegration.

240

241 **4 Discussion**

242 The widespread elevation losses suggested here for both sides of the nAP at high
243 elevations, and especially for the western side of the divide, have significant
244 implications for the region's recent mass change history. Moreover, the detailed
245 mapping on a basin-by-basin scale supports model and GPS studies of local bedrock
246 uplift. A recent study (Neild *et al.*, 2014), using an earlier (near-final) version of our
247 presented data combined with continuous GPS uplift measurements at sites in the

248 Peninsula, modelled both the elastic response and long-term isostatic rebound in
249 the region, showing that the nAP is underlain by very low viscosity mantle.

250

251 Previous observational studies have shown that the elevation decline pattern for ISL
252 or IFL glaciers here and in other similar glaciated regions migrates upstream and
253 diffuses on a scale of years to decades (*Howat et al., 2007; Joughin et al., 2008;*
254 *Shuman et al., 2011; Berthier et al., 2012*), consistent with kinematic wave models of
255 glacier response to ice front stress changes for tidewater glaciers (*Pfeffer, 2007;*
256 *Nick et al., 2009; Favier et al., 2014*). In past work in this area (*Shuman et al., 2011;*
257 *Berthier et al., 2012*), and with comparison to these results, we observe that eastern
258 ISL glaciers are currently propagating kinematic waves upstream from their lower
259 trunk areas, but this process has not yet had a significant impact on higher
260 elevations for the eastern glacier basins. Western-coast nAP glacier front retreats,
261 elevation losses, and accelerations have been documented (*Cook and Vaughan,*
262 *2005; Pritchard and Vaughan, 2007; Kunz et al., 2012; Christ et al., 2014*), with a
263 major pulse of retreat beginning in the 1970s. Moreover, our work here shows that
264 on-going ice front losses within the study period behave much like smaller versions
265 of the eastern-side glaciers impacted by ice shelf and glacier front retreat (Table 1;
266 Figure 2). The earlier losses inferred for the western side fjord glaciers (e.g., *Christ*
267 *et al., 2014*) appear to have now propagated throughout the entirety of the western
268 basins, leading to significant and widespread surface lowering in the western upper
269 catchment areas (>1000 a.s.l.) at greater rates than for the eastern side on average
270 (Table 1 and Table S2).

271

272 However, any measurement of elevation or mass losses along the western coast and
273 in the upper elevation areas must be reconciled with a large recent positive snow
274 accumulation anomaly. Ice cores at two sites on the nAP ridge crest (Detroit Plateau,
275 64.08°S, 59.65°W, 1937 m a.s.l., and Site Beta of the Larsen Ice Shelf System,
276 Antarctica, 66.03°S, 64.04°W, 1980 m a.s.l.; Figure 1) show significant increases in
277 accumulation in the late 20th century: 2052 to 2776 kg m² a⁻¹ from 1981-87 to 2001-
278 07, and 1750 to 2710 kg m² a⁻¹ from 1960-69 to 2000-08, respectively (*Potocki et al.,*

279 2011; Goodwin, 2013). Models of precipitation input for the region (Saha et al.,
280 2010; Dee et al., 2011; Lenaerts et al., 2012) also show a strong overall increase for
281 the most recent decades, but some indicate a slight decline in the last decade,
282 covering our dH/dt measurement period (Saha et al., 2010; Lenaerts et al., 2012;
283 Shepherd et al., 2012). The large increase and later reduction in accumulation are
284 associated with multi-decadal warming (Barrand et al., 2013) and with reductions
285 in sea ice extent northwest of the nAP (Stammerjohn et al., 2012), recently
286 moderated by a slight cooling trend (Blunden and Arndt, 2012; Zagorodnov et al.,
287 2012).

288

289 Multi-decadal accumulation, temperature and snowmelt trends cause changes in the
290 compaction rate of snow and firn, and can potentially impact measurements of
291 surface elevation change (Ligtenberg et al., 2011). Using a model climate time series
292 (based on reanalysis of weather data) spanning the period of our measurements
293 (RACMO-2.1/ANT; Lenaerts et al., 2012), a dH/dt for the firn column at 27 km
294 spatial scale is obtained similar to that used in previous related analyses (Pritchard
295 et al., 2012; Gardner et al., 2013). The modelled inter-annual variability in
296 accumulation, temperature, and snowmelt and their effect on firn compaction result
297 in dH/dt corrections between -0.19 to +0.12 m a⁻¹ on the grounded ice of the nAP,
298 with generally positive (thickening) corrections on the western side and negative to
299 the east. The small effect on the firn layer, and the high variability of accumulation
300 both inter-annually and among the basin areas (Figure 4a) make the correction
301 relatively insignificant. We therefore report dH/dt as observed from the satellite
302 data. From these observations, we report mass change in Table 1 and Table S2 as:

303

304

$$(dH/dt)_{hyps} * (A) * \rho \quad (2)$$

305

306

307

308

309

where $(dH/dt)_{hyps}$ is the elevation-band-weighted mean measured dH/dt, A is area
of the glacier basin or island, and ρ is our assumed mean density of ice and firn lost
by dynamics (900 kg m⁻³). We eliminated the nunatak areas from each of the basins,
based on the Antarctic Digital Database mapping of rock outcroppings in the region

310 similar to previous studies (e.g., *Gardner et al.*, 2013).

311

312 Our estimate of mass balance for the combined nAP region is $-24.9 \pm 7.8 \text{ Gt a}^{-1}$, with
313 the great majority of the mass loss occurring at elevations below 1000 m a.s.l. ($-$
314 $21.9 \pm 6.3 \text{ Gt a}^{-1}$, or 88%; Table 1). Regionally, the eastern nAP basins dominate the
315 mass loss at $-17.7 \pm 3.7 \text{ Gt a}^{-1}$, or 72% of the loss, and of this, $-15.2 \pm 3.2 \text{ Gt a}^{-1}$ (60%) is
316 from 12 glacier basins flowing into embayments formerly occupied by the Prince
317 Gustav, Larsen Inlet, Larsen A, and Larsen B ice shelves. For the 11 western nAP
318 glacier basins and islands, the mass loss rate is similar at low and high elevations ($-$
319 $2.3 \pm 0.7 \text{ Gt a}^{-1}$ $>1000 \text{ m a.s.l.}$, and $-2.2 \pm 1.0 \text{ Gt a}^{-1}$ below). Overall, the nAP region
320 accounts for $\sim 29\%$ of Antarctica mass imbalance during the study period (*Shepherd*
321 *et al.*, 2012).

322

323 We also examined the mass balance ratio of the basins and regional areas, based on
324 mass input, primarily snow accumulation (*Lenaerts et al.*, 2012; Table 2, Table S3).
325 Surface mass balance (SMB) in the region has a very large gradient from west to
326 east, with values of 1500 to 3000 $\text{kg m}^{-2} \text{ a}^{-1}$ for the western areas and high
327 elevations dropping to ~ 500 to 1500 $\text{kg m}^{-2} \text{ a}^{-1}$ in the low elevation areas of the
328 eastern nAP coast. A ratio of the mass balance divided by the mass accumulation
329 input indicates the degree of imbalance in the glacier systems, and suggests the level
330 of ice flux increase for glacier systems having recently accelerated due to ice front or
331 ice shelf losses. We term this value the imbalance ratio. The imbalance ratio for the
332 nAP as a whole is -0.45, implying that mass outflow is 45% greater during the study
333 period relative to a steady-state rate in the current climate. For the eastern nAP
334 glaciers, the mean ratio is -0.8 and the major ISL glaciers in the Larsen A and Larsen
335 B between -0.33 and -3.4. The upper areas of these glacier systems are essentially
336 balanced (ratio ~ -0.1). IFL glaciers along the western and northern coastlines have
337 imbalance ratios similar to the major ISL glaciers, ~ -0.5 to -2.4 .

338

339 Our mass balance estimate for the nAP region agrees well with recently published
340 gravimetric values. Recent GRACE-based estimates that can be most easily

341 compared with our study yield values of $-27.5 \pm 10 \text{ Gt a}^{-1}$ (summing the mascons
342 encompassing and adjacent to our study area) (Luthcke *et al.*, 2013), and $26 \pm 3 \text{ Gt a}^{-1}$
343 for a larger GRACE mascon extending to 70°S (Sasgen *et al.*, 2013). Due to the low
344 spatial resolution of the gravimetric measurement, both these GRACE-derived
345 results inherently include portions of the Larsen C Ice Shelf and adjacent ice-
346 covered islands we did not measure (notably, King George Island) that lost elevation
347 and mass during the ICESat period (Gardner *et al.*, 2013). Similarly, the strong east-
348 west gradient revealed in our study is not discernable by the GRACE system.
349 Overall, however, the GRACE results provide a good summary confirmation for our
350 study, and imply that nearly all of the net mass loss for the Peninsula lies in the nAP
351 region defined here.

352

353 For earlier ICESat-only studies of the mass balance in the area (Shepherd *et al.*,
354 2012), the apparent agreement is likely fortuitous. Simple extrapolation methods
355 that do not include information about individual basin dynamics (e.g.,
356 spatial/elevation extent, ice shelf loss, east-west variations), lead to very different
357 values for total mass change. We conducted two experiments using only our cross-
358 track adjusted ICESat data to examine the scale of possible discrepancies. With an
359 assumption of uniform elevation change for each elevation band *throughout* the
360 nAP, the volume change from ICESat data would be $-36.6 \text{ km}^3 \text{ a}^{-1}$. This overestimate
361 derives from ISL glaciers forming too great a part of the net elevation change
362 measurement data, especially for their lower elevations. This is, in part, due to more
363 ICESat data being acquired along the eastern nAP, likely a result of less cloud cover
364 there. If one partially addresses this by separating ICESat data in two subsets (ISL
365 basins vs the rest), the volume change is still 10% greater than our study, -30.6 km^3
366 a^{-1} .

367

368 The most recent assessment of the mass balance of the entire Peninsula uses
369 CryoSat-2 interferometric radar altimetry data to infer a mass balance of $-13 \pm 13 \text{ Gt}$
370 a^{-1} in the most comparable basins of their study for a period following our
371 evaluation, 2010-2013 (McMillan *et al.*, 2014; their basins 25 and 26). We suggest

372 that the large difference between this study and ours is due to underrepresentation
373 of the narrow deep fjord glaciers on both sides that are rapidly losing ice elevation.
374 This is inherent to the use of a radar altimeter over rough terrain: the system
375 unavoidably oversamples high areas within the beam footprint. However, detailed
376 study of a set of glacier outlets that formerly fed the Larsen A and Prince Gustav ice
377 shelves (which were the site of major ice shelf disintegrations in 1988 and 1995)
378 suggests some parts of our study area have begun to see a slightly reduced level of
379 ice mass loss in the 2011-2013 period (H. Rott, pers. comm., 2014).

380

381 We now examine the potential impact of further ice shelf loss in the Scar Inlet
382 region, a remnant ice shelf section from the Larsen B Ice Shelf. Comparing high-
383 resolution bathymetric mapping of the seabed exposed by nAP-wide ice shelf loss
384 and glacier retreat with our data in Figure 1 shows that it is the glaciers with deep
385 (>500 m) troughs and recent ice shelf loss that have the greatest elevation loss and
386 mass imbalance (Zgur *et al.*, 2007; Shuman *et al.*, 2011; Rebesco *et al.*, 2014). Recent
387 ice-thickness maps of the tributary glaciers (Starbuck, Flask, and Leppard glaciers)
388 of the still-intact Scar Inlet Ice Shelf (SIIS) indicate they have unusually deep glacier
389 troughs just behind the grounding line, well in excess of 1000 m below sea level in
390 the case of Flask Glacier, and 500 m below sea level for Starbuck glacier (Farinotti *et*
391 *al.*, 2013, Farinotti *et al.*, 2014). From Table S3, the mean imbalance ratio of ISL
392 glaciers with ice-front bathymetric troughs exceeding 500 m depth is -1.20, and -
393 3.18 for those exceeding 1000 m depth. (for comparison, it is +0.07 for trough areas
394 less than 500 m depth). If we assume that the three primary tributary glaciers of SIIS
395 will experience the same mean imbalance ratio following a collapse of their frontal
396 ice shelf in Scar Inlet, we can anticipate increased mass imbalance in those basins,
397 from the -1.36 Gt a⁻¹ observed during our study period to ~-5.5 Gt a⁻¹.

398

399 **5 Conclusions**

400 Overall, our study suggests that the nAP mass imbalance pattern is a combination of
401 several recent changes to the coastal glaciers and ice shelf systems, likely beginning
402 several decades ago along the western coastal fjords and islands, with extensive

403 inland propagation of mass loss to the ice divide area, and more recent ice shelf loss
404 along the eastern flanks and islands with extensive and expanding inland
405 propagation. Further, the large measured increase in snow accumulation over the
406 past few decades has not created vast regions of positive mass balance suggesting
407 that negative mass balances will continue into the future.

408

409 **Authorship contributions**

410 *T. Scambos led the writing and compilation of graphics and tables, and with T. Haran and J.*
411 *Bohlander, conducted the ICESat-based elevation change analysis. E. Berthier conducted the*
412 *differential DEM analysis and integrated the ICESat data with the dDEM data. C. Shuman and*
413 *A. Cook evaluated glacier front area changes and C. Shuman produced components of the*
414 *spatial analysis. A. Cook provided the glacier basin outlines. S. Ligtenberg evaluated the firn*
415 *compaction and accumulation variability estimates, and their impact on our results. All co-*
416 *authors contributed to the writing of the paper.*

417

418 **Acknowledgements**

419 The ICESat data for this paper are available at the NASA Distributed Active Archive
420 Center at NSIDC (GLA12 - GLAS/ICESat L2 Antarctic and Greenland Ice Sheet
421 Altimetry Data). The SPOT5 HRS data were provided at no cost by CNES through the
422 SPIRIT project. The ASTER data were provided at no cost by NASA/USGS through
423 the Global Land Ice Measurements from Space (GLIMS) project. This work was
424 supported by NASA grant NNX10AR76G to T. Scambos and W. Abdalati, the TOSCA
425 and ISIS programs of the French Space Agency (CNES) to E. Berthier, NASA
426 Cryospheric Program funds to C. Shuman, NSF grant ANT-0732921 to T. Scambos,
427 and the Netherlands Polar Program and European Union Seventh Framework
428 Programme grant 226375 to S. Ligtenberg.

429

430

431 **References**

432

433 Barrand, N. E., Vaughan, D. G., Steiner, N., Tedesco, M., Kuipers Munneke, P., van den
434 Broeke, M. J., and Hosking, J. S.: Trends in Antarctic Peninsula surface melting

435 conditions from observations and regional climate modeling, *J. Geophys Res.*,
436 118(1), 315–330, doi:10.1029/2012JF002559, 2013.

437 Berthier, E., Scambos, T. A., and Shuman, C. A.: Mass loss of Larsen B tributary
438 glaciers (Antarctic Peninsula) unabated since 2002, *Geophys. Res. Lett.*, 39
439 L13501, doi:10.1029/2012GL051755, 2012.

440 Blunden, J., and Arndt, D. S.: State of the Climate in 2011, *Bull. Amer. Meteor. Soc.*,
441 93(7), S1–S282, doi:10.1175/2012BAMSStateoftheClimate.1., 2012.

442 Christ, A., Talia-Murray, M., Elking, N., Domack, E., Leventer, A., Lavoie, C., Brachfield,
443 S., Yoo, K.-C., Gilbert, R., Jeong, S.-M., Petrushak, S., Wellner, J.: Late Holocene
444 glacial advance and ice shelf growth in Barilari 1 Bay, Graham Land, west
445 Antarctic Peninsula, *Geol. Soc. Am. Bull.*, doi:10.1130/B31035.1, 2014.

446 Cook, A. J., and Vaughan, D. G.: Overview of areal changes of the ice shelves on the
447 Antarctic Peninsula over the past 50 years, *The Cryosphere*, 4(1), 77–98,
448 doi:10.5194/tc-4-77-2010, 2010.

449 Cook, A. J., Fox, A. J., Vaughan, D. G., and Ferrigno, J. G.: Retreating glacier fronts on
450 the Antarctic Peninsula over the past half-century, *Science*, 308(5721), 541–
451 544, 2005.

452 Cook, A. J., Murray, T., Luckman, A., Vaughan, D. G., and Barrand, N. E.: A new 100-m
453 Digital Elevation Model of the Antarctic Peninsula derived from ASTER
454 Global DEM: methods and accuracy assessment, *Earth System Science Data*,
455 4, 129–142, doi:10.5194/essd-4-129-2012, 2012.

456 Dee, D. P., Uppala, S. M., Simmons, A. J., Berrisford, P., Poli, P., Kobayashi, S., Andrae,
457 U., Balmaseda, M. A., Balsamo, G., Bauer, P., Bechtold, P., Beljaars, A. C. M., van
458 de Berg, L., Bidlot, J., Bormann, N., Delsol, C., Dragani, R., Fuentes, M., Geer, A.
459 J., Haimberger, L., Healy, S. B., Hersbach, H., Hólm, E. V., Isaksen, I., Kållberg,
460 P., Köhler, M., Matricardi, M., McNally, A. P., Monge-Sanz, B. M., Morcrette, J.-J.,
461 Park, B.-K., Peubey, C., de Rosnay, P., Tavolato, C., Thépaut, J.-N. and Vitart, F.:
462 The ERA-Interim reanalysis: configuration and performance of the data
463 assimilation system, *Q. Jour. Royal Met. Soc.*, 137(656), 553–597,
464 doi:10.1002/qj.828, 2011.

465 Farinotti, D., Corr, H., and Gudmundsson, G. H.: The ice thickness distribution of
466 Flask Glacier, Antarctic Peninsula, determined by combining radio-echo
467 soundings, surface velocity data and flow modelling, *Ann. Glaciol.*, 54(63),
468 18–24, doi:10.3189/2013AoG63A603, 2013.

469 Farinotti, D., King, E. C., Albrecht, A., Huss, M., and Gudmundsson, G. H.: The bedrock
470 topography of Starbuck Glacier, Antarctic Peninsula, as measured by radio-
471 echo sounding, *Ann. Glaciol.*, 55(67), 22–28, doi:10.3189/2014AoG67A025,
472 2014.

- 473 Favier, L., Durand, G., Cornford, S. L., Gudmundsson, G. H., Gagliardini, O., Gillet-
474 Chaulet, F., Zwinger, T., Payne, A. J., and Le Brocq, A. M.: Retreat of Pine Island
475 Glacier controlled by marine ice-sheet instability, *Nature Clim. Change*, 4(2),
476 117–121, doi:10.1038/nclimate2094, 2014
- 477 Flament, T., and Rémy, F.: Dynamic thinning of Antarctic glaciers from along-track
478 repeat radar altimetry, *J. Glaciol.*, 58(211), 830–840,
479 doi:10.3189/2012JoG11J118, 2012.
- 480 Fujisada, H., Bailey, G. B., Kelly, G. G., Hara, S., and Abrams, M. J.: ASTER DEM
481 performance, *IEEE T. Geosci. Remote Sens.*, 43(12), 2707–2714, 2005
- 482 Gardelle, J., Berthier, E., Arnaud, Y., and Käab, A.: Region-wide glacier mass balances
483 over the Pamir-Karakoram-Himalaya during 1999–2011, *The Cryosphere*, 7,
484 1263–1286, doi:10.5194/tc-7-1263-2013, 2013.
- 485 Gardner, A. S., Moholdt, G., Cogley, J. G., Wouters, B., Arendt, A. A., Wahr, J., Berthier,
486 E., Hock, R., Pfeffer, W. T., Kaser, G., Ligtenberg, S. R. M., Bolch, T., Sharp, M. J.,
487 Hagen, J. O., van den Broeke, M. R., and Paul, F.: A Reconciled Estimate of
488 Glacier Contributions to Sea Level Rise: 2003 to 2009, *Science*, 340(6134),
489 852–857, doi:10.1126/science.1234532, 2013.
- 490 Goodwin, B. P.: Recent Environmental Changes on the Antarctic Peninsula as
491 Recorded in an ice core from the Bruce Plateau. PhD diss., The Ohio State
492 University, Columbus, OH, 247 pp., 2013.
- 493 Haran, T., Bohlander, J., Scambos, T. and Fahnestock, M.: MODIS Mosaic of Antarctica
494 2004 (MOA2004) Image Map. Boulder, Colorado USA: National Snow and Ice
495 Data Center, doi:10.7265/N5ZK5DM5, 2005, updated 2014.
- 496 Haran, T., Bohlander, J., Scambos, T., Painter, T., and Fahnestock, M.: MODIS Mosaic
497 of Antarctica 2008-2009 (MOA2009) Image Map. Boulder, Colorado USA:
498 National Snow and Ice Data Center, doi:10.7265/N5KP8037, 2014.
- 499 Howat, I. M., Joughin, I., and Scambos, T. A.: Rapid Changes in Ice Discharge from
500 Greenland Outlet Glaciers, *Science*, 315(5818), 1559–1561, 2007.
- 501 Ivins, E. R., Watkins, M. M., Yuan, D.-N., Dietrich, R., Casassa, G., and Rülke, A.: On-
502 land ice loss and glacial isostatic adjustment at the Drake Passage: 2003–
503 2009, *J. Geophys. Res.-Earth*, 116, B02403, doi:10.1029/2010JB007607,
504 2011.
- 505 Joughin, I., Howat, I. M., Fahnestock, M., Smith, B., Krabill, W., Alley, R. B., Stern, H.,
506 and Truffer, M.: Continued evolution of Jakobshavn Isbrae following its rapid
507 speedup, *J. Geophys. Res.-Earth*, 113, F04006, doi:10.1029/2008JF001023,
508 2008.

- 509 Korona, J., Berthier, E., Bernard, M., Rémy, F., and Thouvenot, E.: SPIRIT. SPOT 5
510 stereoscopic survey of Polar Ice: Reference Images and Topographies during
511 the fourth International Polar Year (2007-2009), *ISPRS J. Photogramm.*, 64,
512 204–212, doi:10.1016/j.isprsjprs.2008.10.005, 2009.
- 513 Kunz, M., King, M. A., Mills, J. P., Miller, P. E., Fox, A. J., Vaughan, D. G., and Marsh, S.
514 H.: Multi-decadal glacier surface lowering in the Antarctic Peninsula,
515 *Geophys. Res. Lett.*, L19502, 10.1029/2012GL052823, 2012.
- 516 Lenaerts, J. T. M., van den Broeke, M. R., van de Berg, W. J., van Meijgaard, E., and
517 Munneke, P. K.: A new, high-resolution surface mass balance map of
518 Antarctica (1979-2010) based on regional atmospheric climate modeling,
519 *Geophys. Res. Lett.*, 39, L04501, 4501–4501, doi:10.1029/2011GL050713,
520 2012.
- 521 Ligtenberg, S. R. M., Helsen, M. M., and van den Broeke, M. R.: An improved semi-
522 empirical model for the densification of Antarctic firn, *The Cryosphere*, 5(4),
523 809–819, doi:10.5194/tc-5-809-2011, 2011.
- 524 Luthcke, S. B., Sabaka, T. J., Loomis, B. D., Arendt, A. A., McCarthy, J. J., and Camp, J.:
525 Antarctica, Greenland and Gulf of Alaska land-ice evolution from an iterated
526 GRACE global mascon solution, *J. Glaciol.* 59, 613–631,
527 doi:10.3189/2013JoG12J147, 2013.
- 528 McMillan, M., Shepherd, A., Sundal, A., Briggs, K., Muir, A., Ridout, A., Hogg, A., and
529 Wingham, D.: Increased ice losses from Antarctica detected by CryoSat-2,
530 *Geophys. Res. Lett.* 41, 1-7, doi:10.1002/2014GL060111, 2014.
- 531 Mulvaney, R., Abram, N. J., Hindmarsh, R. C., Arrowsmith, C., Fleet, L., Triest, J., ... &
532 Foord, S.: Recent Antarctic Peninsula warming relative to Holocene climate
533 and ice-shelf history, *Nature* 489(7414), doi:10.1038/nature11391, 141-
534 144., 2012.
- 535 Nick, F. M., Vieli, A., Howat, I. M., and Joughin, I.: Large-scale changes in Greenland
536 outlet glacier dynamics triggered at the terminus, *Nature Geosci.*, 2(2), 110–
537 114, 2009.
- 538 Nield, G. A., Barletta, V. R., Bordoni, A., King, M. A., Whitehouse, P. L., Clarke, P. J.,
539 Domack, E., Scambos, T., and Berthier, E.: Rapid bedrock uplift in the
540 Antarctic Peninsula explained by viscoelastic response to recent ice
541 unloading, *Earth and Planetary Science Letters*, 397, doi:
542 10.1016/j.epsl.2014.04.019, 32-41, 2014.
- 543 Pfeffer, W. T.: A simple mechanism for irreversible tidewater glacier retreat, *J.*
544 *Geophys. Res.-Earth*, 112 (F3), F03S25, doi:10.1029/2006JF000590, 2007.

- 545 Potocki, M., Mayewski, P. A., Kurbatov, A., Handley, M., Simoes, J. C., and Jaña, R.:
546 Detailed glaciochemical records from a northern Antarctic Peninsula site-
547 Detroit Plateau. In AGU Fall Meeting Abstracts, 1, p. 1822, 2011, San
548 Francisco, 5-9 December, 2011.
- 549 Pritchard, H. D., and Vaughan, D. G.: Widespread acceleration of tidewater glaciers
550 on the Antarctic Peninsula, *J Geophys Res-Earth*, 112(F3), F03S29,
551 doi:10.1029/2006JF000597, 2007.
- 552 Pritchard, H. D., Arthern, R. J., Vaughan, D. G., and Edwards, L. A.: Extensive dynamic
553 thinning on the margins of the Greenland and Antarctic ice sheets, *Nature*,
554 461(7266), 971–975, 2009.
- 555 Pritchard, H. D., Ligtenberg, S. R. M., Fricker, H. A., Vaughan, D. G., van den Broeke, M.
556 R., and Padman, L.: Antarctic ice-sheet loss driven by basal melting of ice
557 shelves, *Nature*, 484(7395), 502–505, doi:10.1038/nature10968, 2012.
- 558 Rebesco, M., Domack, E., Zgur, F., Leventer, A., Lavoie, C., Brachfeld, S., Willmott, V.,
559 Halverson, G., Truffer, M., Scambos, T., Smith, J., and Pettit, E.: Boundary
560 condition of grounding lines prior to collapse, Larsen-B Ice Shelf, *Antarctica*.
561 *Science* 345(6202), doi:10.1126/science.1256697, 2014.
- 562 Rignot, E., Casassa, G., Gogineni, P., Krabill, W., Rivera, A., and Thomas, R.:
563 Accelerated ice discharge from the Antarctic Peninsula following the collapse
564 of Larsen B ice shelf, *Geophys. Res. Lett.*, 31, L18401, 2004.
- 565 Rignot, E., Bamber, J. L., van den Broeke, M. R., Davis, C., Li, Y. H., van de Berg, J., and
566 van Meijgaard, E.: Recent Antarctic ice mass loss from radar interferometry
567 and regional climate modelling, *Nat. Geosci.*, 1(2), 106–110,
568 doi:10.1038/ngeo102, 2008.
- 569 Rott, H., Müller, F., Nagler, T., and Floricioiu, D.: The imbalance of glaciers after
570 disintegration of Larsen B ice shelf, Antarctic Peninsula, *The Cryosphere*,
571 5(1), 125–134, doi:10.5194/tc-5-125-2011, 2011.
- 572 Saha, S., Moorthi, S., Wu, X., Wang, J., Nadiga, S., Tripp, P., Behringer, D., Hou, Y.-T.,
573 Chuang, H.-Y., Iredell, M., Ek, M., Meng, J., Yang, R., Mendez, M. P., van den
574 Dool, H., Zhang, Q., Wang, W., Chen, M., Becker, E. (2013). The NCEP climate
575 forecast system version 2. *Journal of Climate*, 27, doi:10.1175/JCLI-D-12-
576 00823.1, 2013.
- 577 Sasgen, I., H. Konrad, E. R. Ivins, M. R. Van den Broeke, J. L. Bamber, Z. Martinec, and
578 V. Klemann (2013), Antarctic ice-mass balance 2003 to 2012: regional
579 reanalysis of GRACE satellite gravimetry measurements with improved
580 estimate of glacial-isostatic adjustment based on GPS uplift rates, *The*
581 *Cryosphere*, 7(5), 1499–1512, doi:10.5194/tc-7-1499-2013, 2013.

- 582 Scambos, T. A., Haran, T. M., Fahnestock, M. A., Painter, T. H., and Bohlander, J.:
583 MODIS-based Mosaic of Antarctica (MOA) data sets: Continent-wide surface
584 morphology and snow grain size, *Remt. Sens. Environ.*, 111(2), 242-257,
585 2007.
- 586 Schutz, B. E., Zwally, H. J., Shuman, C. A., Hancock, D., and DiMarzio, J. P. : Overview of
587 the ICESat mission. *Geophys. Res. Lett.*, 32(21), L21S01, doi:
588 10.1029/2005GL024009, 2005.
- 589 Shepherd, A., Ivins, E. R., A, G., V. R., Bentley, M. J., Bettadpur, S., Briggs, K., Bromwich,
590 D. H., Forsberg, R., Galin, N., Horwath, M., Jacobs, S., Joughin, I., King, M. A.,
591 Lenaerts, J. T. M., Li, J., Ligtenberg, S. R. M., Luckman, A., Luthcke, S. B.,
592 McMillan, M., Meister, R., Milne, G., Mouginot, J., Muir, A., Nicolas, J. P., Paden,
593 J., Payne, A. J., Pritchard, H., Rignot, E., Rott, H., Sørensen, L. S., Scambos, T. A.,
594 Scheuchl, B., Schrama, E. J. O., Smith, B., Sundal, A. V., J. H., van de Berg, W. J.,
595 van den Broeke, M. R., Vaughan, D. G., Velicogna, I., Wahr, J., Whitehouse P. L.,
596 Wingham, D. J., Yi, D., Young, D., and Zwally, H. J.: A Reconciled Estimate of
597 Ice-Sheet Mass Balance, *Science*, 338(6111), 1183–1189,
598 doi:10.1126/science.1228102, 2012.
- 599 Shuman, C. A., Zwally, H. J., Schutz, B. E., Brenner, A. C., DiMarzio, J. P., Suchdeo, V. P.,
600 and Fricker, H. A.: ICESat Antarctic elevation data: preliminary precision and
601 accuracy assessment, *Geophys. Res. Lett.* 33(7), L07501, doi:
602 10.1029/2005GL025227, 2007.
- 603 Shuman, C. A., Berthier, E., and Scambos, T. A.: 2001-2009 elevation and mass losses
604 in the Larsen A and B embayments, Antarctic Peninsula, *J. Glaciol.*, 57(204),
605 737–754, doi:10.3189/002214311797409811, 2011.
- 606 Stammerjohn, S. E., D. G. Martinson, R. C. Smith, X. Yuan, and D. Rind, D.: Trends in
607 Antarctic annual sea ice retreat and advance and their relation to El Niño–
608 Southern Oscillation and Southern Annular Mode variability, *J. Geophys. Res.*
609 *Oceans* (1978–2012), 113(C3), C03S90, doi: 10.1029/2007JC004269, 2008.
- 610 van den Broeke, M.,: Strong surface melting preceded collapse of Antarctic Peninsula
611 ice shelf, *Geophys. Res. Lett.*, 32(12), L12815, doi:10.1029/ 2005GL023247,
612 2005.
- 613 Zagorodnov, V., Nagornov, O., Scambos, T. A., A. Muto, A., Mosley-Thompson, E.,
614 Pettit, E. C., and Tyufin, S.: Borehole temperatures reveal details of 20th
615 century warming at Bruce Plateau, Antarctic Peninsula, *The Cryosphere*, 6(3),
616 675–686, doi:10.5194/tc-6-675-2012, 2012.
- 617 Zgur, F., Rebesco, M., Domack, E. W., Leventer, A., Brachfeld, S., and Willmott, V.:
618 Geophysical survey of the thick, expanded sedimentary fill of the new-born
619 Crane fjord (former Larsen B Ice Shelf, Antarctica), *US Geol. Surv. Open File*
620 *Rep 1047*, 2007.

621 Zwally, H., Schutz, R., Hancock, D., and Dimarzio, J., GLAS/ICESat L2 Antarctic and
622 Greenland Ice Sheet Altimetry Data (HDF5). Version 33. Boulder, Colorado
623 USA: NASA DAAC at the National Snow and Ice Data Center,
624 doi:10.5067/ICESAT/GLAS/DATA205, 2012.

625

626 **Table 1. Summary of Mass Balance for the northern Antarctic Peninsula, 2003-2008[†]**
 627 Units: Area (km²), Mean dM/dt (Gt a⁻¹), Number of Measurements, Mean dH/dt (m a⁻¹), Mean dV/dt (km³ a⁻¹)

628	629	Region	Ice-Covered Area	Total dM/dt ^a	Ice Front Retreat			Below 1000 m a.s.l.				Above 1000 m a.s.l.				
					Area ^b	dH/dt ^c	dV/dt ^{d,h}	Area	dDEM ^e	ICESat ^f	dH/dt ^g	dV/dt ^h	Area	ICESat ^f	dH/dt ^g	dV/dt ^h
630	631	nAP <66°S, 1-33	34222.8	-24.9	325.6	-7.4	-1.2	23571.7	44.8	12476	-1.00	-23.1	10651.7	2668	-0.31	-3.4
632	632	nAP West, 1-11	14338.2	-4.7	7.8	-3.9	-0.0	9014.3	38.6	2999	-0.27	-2.4	5323.7	893	-0.59	-2.8
633	633	nAP North, 12-14	3688.0	-2.3	4.0	-3.7	-0.0	3684.3	8.2	2204	-0.69	-2.5	3.7	(0)	(-0.31)	0.0
634	634	nAP East, 15-33	16196.4	-18.0	313.8	-7.5	-1.2	10872.9	62.4	7279	-1.67	-18.2	5323.5	1775	-0.10	-0.6
635	635	Northwest AP Coast ⁱ	5255.1	-1.7	--	--	--	3417.9	35.1	1270	-0.27	0.9	1837.0	575	-0.50	-0.9
636	636	Western IFL Glaciers ^j	679.4	-1.1	11.8	-4.6	-0.0	452.1	35.6	450	-2.24	-1.0	226.5	(0)	-0.84	-0.2
637	637	Eastern ISL Glaciers ^k	9251.0	-15.2	305.7	-7.7	-1.1	6030.9	70.9	3903	-2.60	-15.7	3232.6	941	-0.01	-0.2
638	638	James Ross Island ^l	1800.8	-2.4	47.1	-3.3	-0.1	1380.0	58.0	417	-1.93	-2.7	420.7	215	0.02	0.0
639	639	Prince Gustav tributaries ^m	1885.0	-2.7	58.2	-3.6	-0.1	1478.4	76.6	475	-2.03	-3.0	406.7	123	0.23	0.1
640	640	Larsen A tributaries ⁿ	3184.4	-4.5	29.3	-2.7	-0.0	2094.8	85.5	1594	-2.32	-4.9	1089.7	329	-0.08	-0.1
641	641	Larsen B ISL tributaries ^o	4181.6	-8.0	218.2	-9.5	-1.0	2457.7	55.2	1834	-3.18	-7.8	1736.2	489	-0.13	-0.2
642	642	Scar Inlet Ice Shelf trib. ^p	3524.5	-1.4	--	--	--	2089.8	46.4	1965	-0.47	-0.7	1434.7	715	-0.37	-0.5

643 [†]Data from ICESat and satellite stereo-image differencing. ICESat data span September 2003 – March 2008. Stereo-image DEMs span 2001 to 2010.
 644 Abbreviations for place names: nAP, northern Antarctic Peninsula; ISL, ice shelf loss; IFL, ice front loss.
 645 ^aAssuming mean density of 900 kg/m³ for all dV/dt measurements. Errors for these values are 0.9 times the sum of errors for dV/dt for each row.
 646 ^bArea determined from additional ASTER, SPOT, and Landsat images, spanning 2000-2002 to 2009-2010
 647 ^cRate of elevation loss measured for the first 50 m elevation band above area of grounded ice retreat.
 648 ^dVolume loss assumes flotation was reached midway between 2001 – 2010 (period of observations).
 649 ^ePercent area covered by differential DEM satellite stereo-image data
 650 ^fNumber of repeat-track point measurements used. If <20 ICESat dH/dt measurements are available, the regional mean ICESat dH/dt for areas > 1000 m
 651 (-0.31 m a⁻¹) or, for sub-basins, the main basin mean, is used.
 652 ^gHypsometric weighting for areas below 1000 m elevation.
 653 ^hErrors on dV/dt can be determined by: ±0.3 m a⁻¹ * area for regions ≤1000 m a.s.l. (dDEM and ICESat data) and ±0.15 ma⁻¹ * area for regions >1000 m a.s.l.
 654 (ICESat data)
 655 ⁱGlacier basins 8 – 11
 656 ^jGlacier basins 1a, 4a, 6a, and 12a. Used dDEM data for >1000 m a.s.l. dH/dt estimate
 657 ^kGlacier basins 19, 21-25, 26b, 27-30, and 31a.
 658 ^lGlacier basins 17, 18, and 19
 659 ^mGlacier basins 19 and 21
 660 ⁿGlacier basins 22-25
 661 ^oGlacier basins 26b, 27-30, and 31a
 662 ^pGlacier basins 31b, 32, and 33

667 **Table 2. Comparison of total mass balance (dM/dt), input surface mass (dM_i/dt), and**
 668 **resulting imbalance ratio.**

669 Units: Area, km²; dM/dt, Gt a⁻¹; Mean dH/dt, m a⁻¹; SMB, kg m⁻² a⁻¹; dM_i/dt, Gt a⁻¹

670	671	672	673	674	675	676	677	678	679	680	681	682	683	684	685	686	687	688	689	690	691	692
Region	Ice-Covered Area	Total dM/dt	Mean dH/dt	Mean SMB	Total dM _i /dt	Imbal. ratio	<1000 dH/dt	<1000 SMB	<1000 dM _i /dt	<1000 ratio	>1000 dH/dt	>1000 SMB	>1000 dM _i /dt	>1000 ratio								
nAP <66°S, 1-33	34222.8	-24.9	-0.81	1543	54.2	-0.45	-1.00	1295	29.9	-0.70	-0.31	2104	23.1	-0.18								
nAP West, 1-11	14338.2	-4.7	-0.37	2112	30.4	-0.14	-0.27	1964	17.7	-0.12	-0.59	2361	12.6	-0.17								
nAP North, 12-14	3688.0	-2.3	-0.69	537	2.0	-1.15	-0.69	537	2.0	-1.15	(-0.31)	920	0.0	--								
nAP East, 15-33	16196.4	-18.0	-1.23	1268	21.8	-0.81	-1.75	1007	10.5	-1.56	-0.10	1844	9.8	-0.06								
Northwest AP Coast ^a	5255.1	-1.7	-0.35	2012	10.6	-0.16	-0.27	1770	6.0	0.13	-0.51	2458	4.5	-0.18								
Western IFL Glaciers ^b	679.4	-1.1	-1.77	1839	1.2	-1.26	-2.24	1484	0.7	-1.29	-0.83	2546	0.6	-0.28								
Eastern ISL Glaciers ^c	9251.0	-15.2	-1.64	1399	13.0	-1.15	-2.60	1143	6.9	-2.05	-0.07	1898	6.1	-0.04								
James Ross Island ^d	1800.8	-2.4	-1.44	689	1.2	-2.09	-1.93	653	0.9	-2.70	0.02	834	0.4	0.00								
Prince Gustav trib. ^e	1885.0	-2.7	-1.54	1173	2.2	-1.23	-2.03	968	1.4	-1.93	0.21	2003	0.8	0.10								
Larsen A tributaries ^f	3184.4	-4.5	-1.55	1624	5.2	-0.94	-2.32	1358	2.8	-1.58	-0.08	2154	2.3	-0.03								
Larsen B ISL trib. ^g	4181.6	-8.0	-1.80	1329	5.6	-1.42	-3.18	1064	2.6	-2.68	-0.13	1713	3.0	-0.07								
Scar Inlet Ice Shelf trib. ^h	3524.5	-1.4	-0.42	1296	4.6	-0.30	-0.47	787	1.6	-0.38	-0.37	2049	2.9	-0.16								

684 ^aGlacier basins 8 – 11
 685 ^bGlacier basins 1a, 4a, 6a, and 12a
 686 ^cGlacier basins 19, 21-25, 26b, 27-30, and 31a
 687 ^dGlacier basins 17, 18, and 19
 688 ^eGlacier basins 19 and 21
 689 ^fGlacier basins 22-25
 690 ^gGlacier basins 26b, 27-30, and 31a
 691 ^hGlacier basins 31b, 32, and 33

693 **Figures**

694

695 Figure 1. Location and outline of basins and sub-basins in the study area, and sites of
696 two ice cores discussed in the text. Region names, basin numbers, and abbreviations
697 are the same as in Table S2 and S3. Major drainage basins evaluated by the study are
698 outlined in white, sub-basins are indicated in blue. Base image is the MODIS Mosaic
699 of Antarctica (Scambos et al., 2007). Inset, location of the study area shown in Figure
700 2.

701

702 Figure 2. Elevation change rates (dH/dt) and major and minor glacier basin or
703 islands for the northern Antarctic Peninsula study area. Cyan outlines indicate the
704 measured study basins and islands; surrounding numbers and letters refer to Table
705 S2 and S3 entries. Magenta outlines with lower-case labels identify sub-basins
706 within a major basin where a separate hypsometric interpolation is used. Black
707 contour line indicates 1000 m a.s.l. elevation. Major ice shelf retreat areas since
708 1980 (Cook and Vaughan, 2010) are indicated in grey-blue, with years of major
709 collapse events and the limit of extensive grounded ice loss shown. Ice edge is from
710 a 2009 MODIS mosaic (Haran et al., 2014).

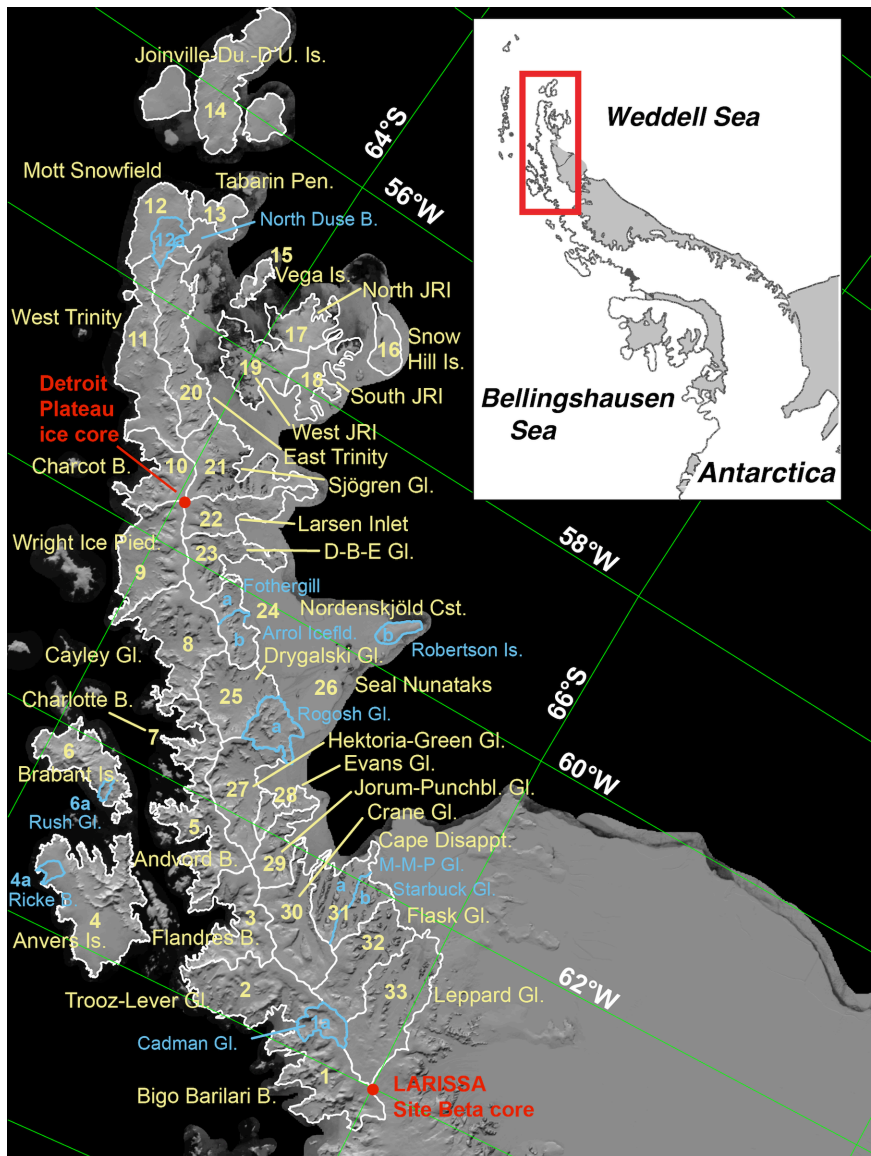
711

712 Figure 3 a-f. Hypsometry of elevation and volume changes of western basins (panel
713 a and b; basins 1 – 11 in Table 1), eastern basins with major ice shelf loss in the
714 period 1986 – 2009 (panels c and d; basins 19, 21-25, and 27-30 in Table 1), and
715 basins draining to the Scar Inlet ice shelf area (panels e and f; basins 31b, 32, and 33
716 in Table 1). Height is binned in 50 m intervals. Note that rates of elevation change
717 trends at the highest elevations (>2000 m a.s.l., right side of left column of panels)
718 are based on few data and are not reliable.

719

720 Figure 4. Comparison of the study area basin extents with RACMO-2 estimated SMB
721 in $\text{kg m}^{-2} \text{a}^{-1}$ (panel a) and mass imbalance ratio for the basin areas separated by
722 high and low elevation areas (above and below 1000 m; panel b).

723



724

725 **Figure 1.** Locations and outlines of basins and sub-basins in the study area, and sites of two
 726 climate ice cores discussed in the text. Region names, basin numbers, and abbreviations are
 727 the same as in Tables S2 and S3. Major drainage basins are outlined in white, sub-basins are
 728 indicated in blue. Base image is the MODIS Mosaic of Antarctica (MOA2004; Scambos *et al.*,
 729 2007; Haran *et al.*, 2005). Inset, location of the study area shown in Figure 2.

730

731

732

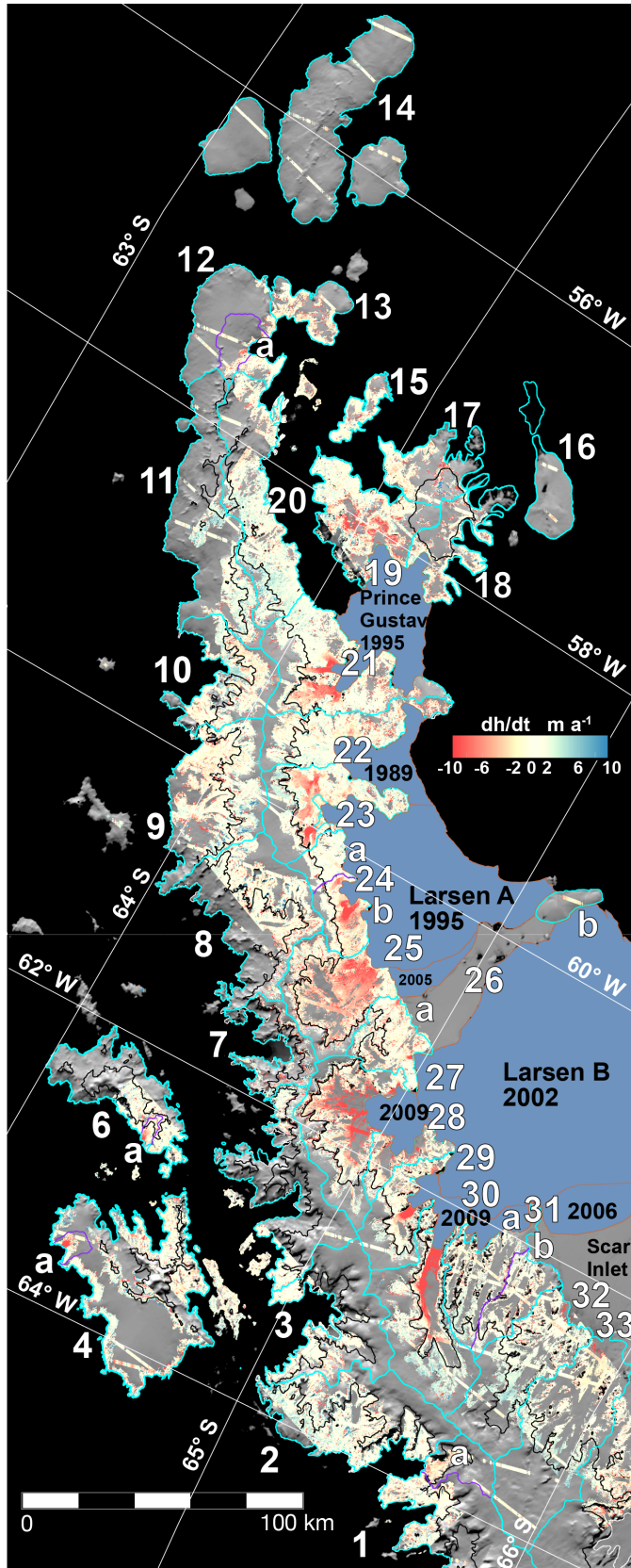
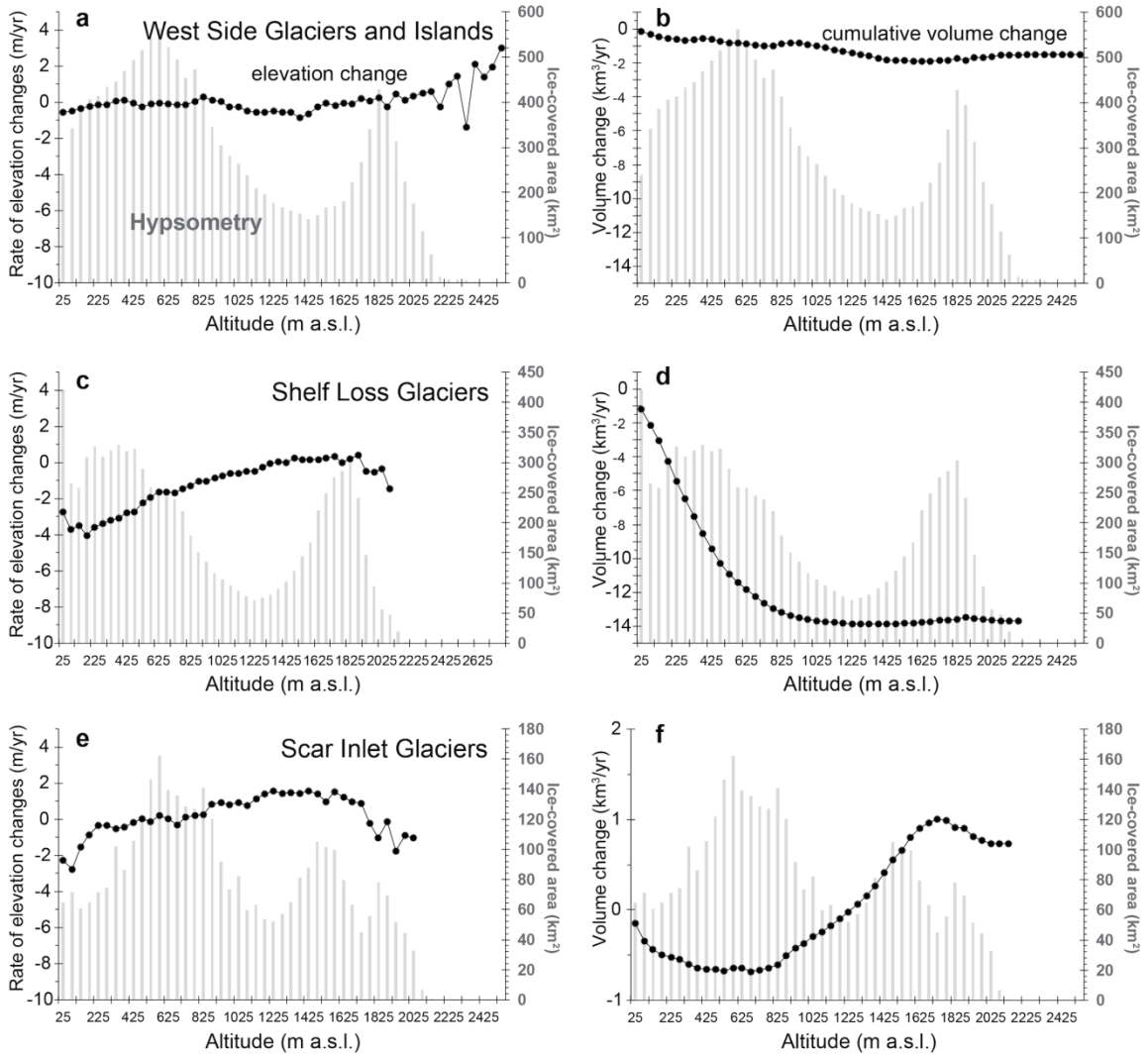


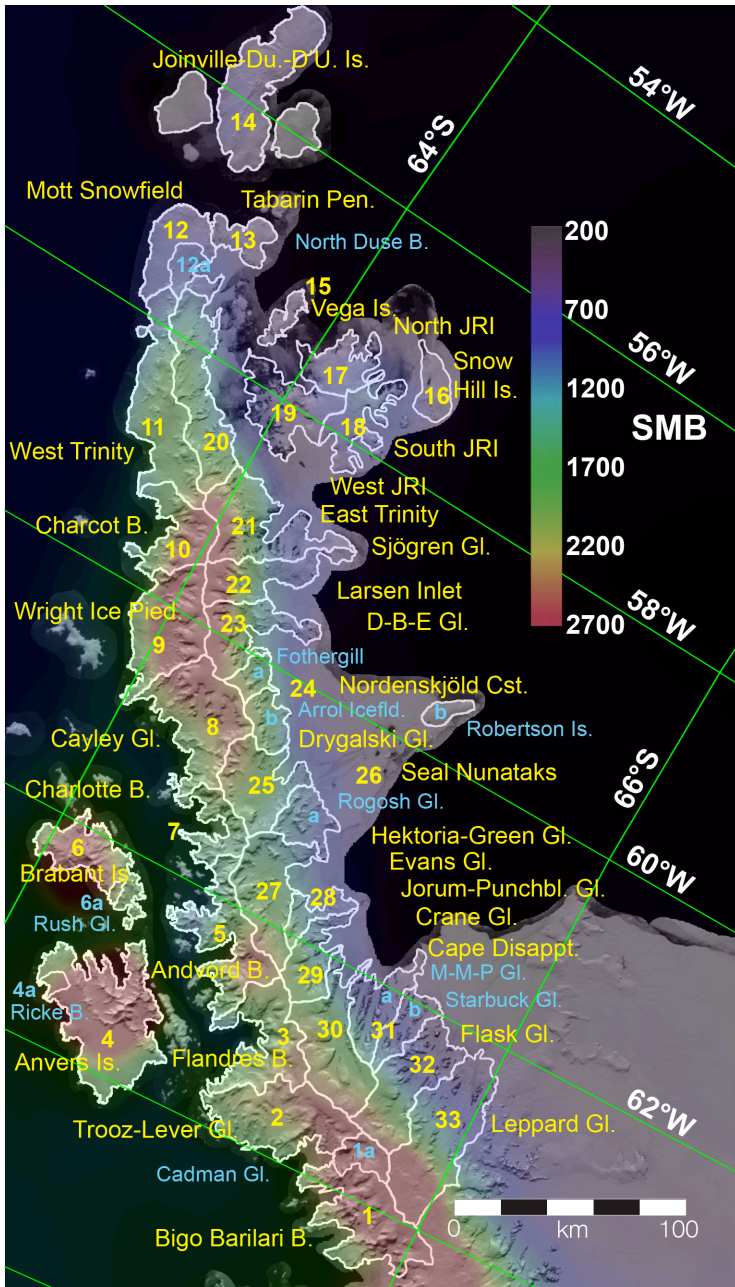
Figure 2. Elevation change rates (dh/dt) and major and minor glacier basin or islands for the northern Antarctic Peninsula study area. Cyan outlines indicate the measured study basins and islands; adjacent numbers and letters refer to Table S2 and S3 entries. Magenta outlines with lower-case labels identify sub-basins within a major basin where a separate hypsometric interpolation is used. A black line indicates the 1000 m a.s.l. elevation contour. Major ice shelf retreat areas since 1980 (*Cook and Vaughan, 2010*) are indicated in blue, with years of major collapse events and the limit of extensive grounded ice loss shown. Ice edge is from a 2009 MODIS mosaic (MOA2009; *Haran et al., 2014*).

734
735
736



737
738
739
740
741
742
743
744
745

Figure 3 a-f. Hypsometry of elevation and volume changes of western nAP basins (panel a and b; basins 1 – 11 in Table S2 and S3), eastern nAP basins with major ice shelf loss in the period 1986 – 2009 (panels c and d; basins 19, 21-25, and 27-30 in Table S2 and S3), and basins draining to the Scar Inlet ice shelf area (panels e and f; basins 31b, 32, and 33 in Tables 1 and 2 and Tables S2 and S3). Height is binned in 50 m intervals. Rates of elevation change trends at the highest elevations (>2000 m a.s.l., right side of left column of panels) are based on few data and are not reliable.



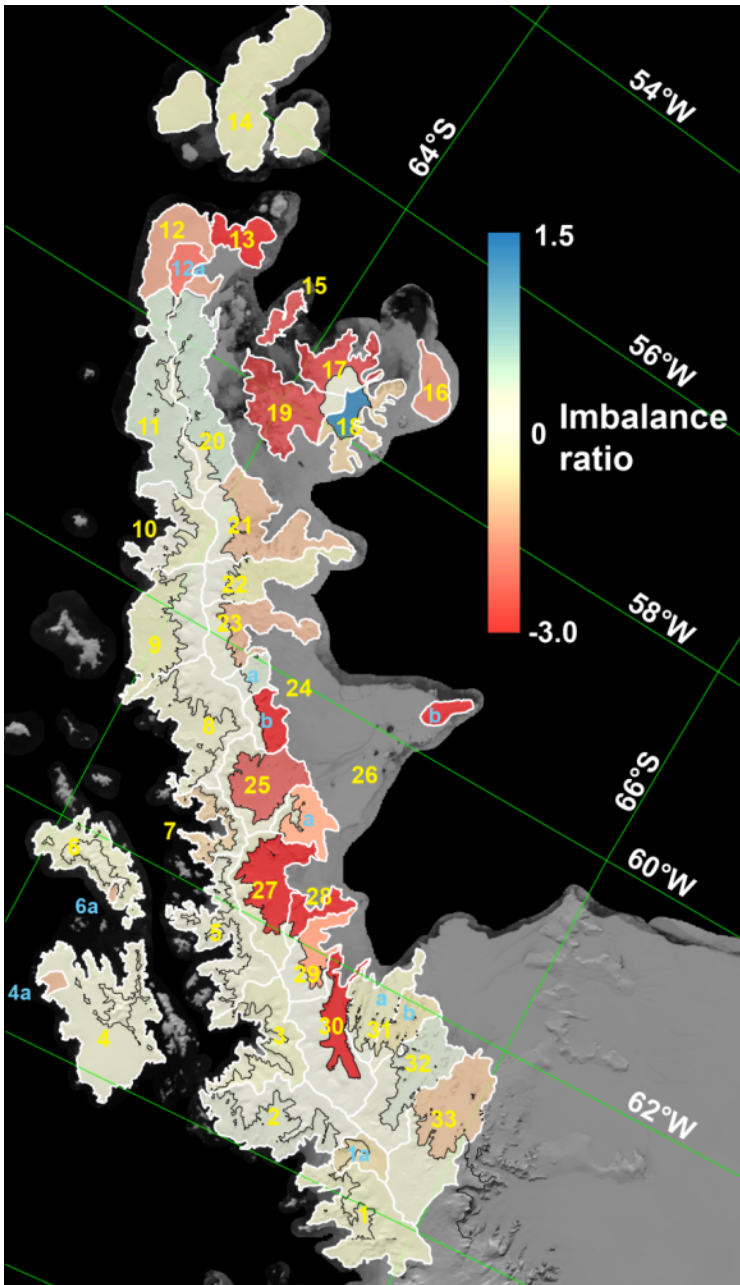
746

747 **Figure 4a.**

748 **Figure 4 a and b.** Comparison of the study area basin extents with RACMO-2
 749 estimated SMB in kg m⁻² a⁻¹ (a) and mass imbalance ratio for the basin areas
 750 separated by high and low elevation areas (above and below 1000 m; b).

751

752



753

754 **Figure 4b**

755 **Figure 4 a and b.** Comparison of the study area basin extents with RACMO-2
 756 estimated SMB in $\text{kg m}^{-2} \text{a}^{-1}$ (a) and mass imbalance ratio for the basin areas
 757 separated by high and low elevation areas (above and below 1000 m; b).